The structure of the photon and its interactions*

Bernd Surrow

CERN, EP-division/OPAL
CH-1211 Geneva 23, Switzerland
E-mail: Bernd.Surrow@cern.ch

Abstract

The OPAL experiment at LEP has performed a variety of measurements of $\gamma\gamma$ and eγ scattering at the e^+e^- collider LEP to gain a deeper insight into the structure of the photon and its interactions. This review presents a summary of these results.

1 Introduction

The photon plays the fundamental role as the gauge boson of mediating electromagnetic interactions through the coupling to charged particles. The photon appears to be in this respect as a point-like particle (Figure 1 (a)). However, a photon is subject to quantum fluctuations, as denoted in Figure 1. It can fluctuate into a lepton/anti-lepton pair, $l\bar{l}$, or a quark/anti-quark pair, $q\bar{q}$ (Figure 1 (b) and (c)). If, e.g in γp interactions, the fluctuation time is large compared to the interaction time, γp interactions can proceed through the interaction of a $q\bar{q}$ pair and the proton, which gives rise to a hadronic type reaction [1]. This behavior has been incorporated in the vector dominance model (VDM) [2] which describes γp interactions as the interaction of the proton and a vector meson resulting from a quantum fluctuation of the photon with the vector meson state having the same quantum numbers as the photon, i.e. $J^{PC} = 1^{--}$. This dual nature of the photon, i.e. point-like and hadron-like, leads to a variety of phenomena which have been investigated in γp and $\gamma\gamma$/eγ[1] scattering at several experiments at HERA and LEP, respectively [3]. The underlying kinematics at the e^+e^- collider LEP is shown in Figure 2. The initial state consists of the incoming electron and positron, each of which - to lowest order in $\alpha_{\rm em}$ - emits a virtual photon. The square of the four momentum transfer or the virtuality of the mediated virtual photons is denoted by $Q^2 = -q^2 = (k_1 - k_1')^2$, which will be later referred to as the probe virtuality,

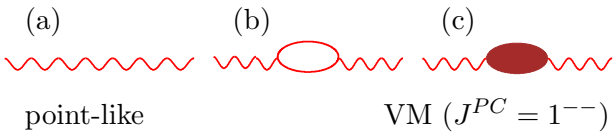

Figure 1: *Dual nature of the photon.*

*Invited talk given at the Workshop on Photon Interactions and the Photon Structure, Lund, Sweden, September 10-13, 1998.

[1]Positrons are referred to as electrons in this review unless otherwise stated.

and $P^2 = -p^2 = (k_2 - k_2')^2$ which will be later referred to as the target virtuality. Q^2 (P^2) can be reconstructed from the energy and angle of the respective detected (tagged) electron as follows: $Q^2 = 2E_{\text{beam}}E_{\text{tag},1}(1 - \cos\theta_{\text{tag},1})$ ($P^2 = 2E_{\text{beam}}E_{\text{tag},2}(1 - \cos\theta_{\text{tag},2})$). The invariant mass of the final state X is denoted by $W = (q + p)^2$. The Bjorken scaling variable x is defined as $x = Q^2/(Q^2 + P^2 + W^2)$ and the 'inelasticity' as $y = (p \cdot q)/(p \cdot k)$. The inelasticity can be reconstructed from the energy and angle of the tagged electron as follows: $y = 1 - E_{\text{tag},1}/E_{\text{beam}}(\cos^2\theta_{\text{tag},1}/2)$.

Three event classes can be distinguished depending on whether the electron in the final state is tagged or not. If both final state electrons are not tagged, both virtualities Q^2 and P^2 - depending on the detector acceptance - are small, and the photons can be considered as quasi-real, i.e. $Q^2 \simeq 0$ and $P^2 \simeq 0$. This is the case of anti-tagged events which allows to investigate $\gamma\gamma$ scattering and thus photon interactions. If one of the scattered electrons, is detected (tagged), the process shown in Figure 2 can be considered as the scattering of an electron off a quasi-real photon. In this case of $e\gamma$ scattering (single-tagged events) one is able to study the photon structure similarly to the case of lepton-nucleon scattering ($Q^2 \gg P^2$). The case in which both final state electrons are tagged is referred to as double-tagged events.

Unlike to ep and γp scattering e.g. at HERA, the invariant mass W and therefore x in eγ and $\gamma\gamma$ scattering at LEP can only be reconstructed from the final state X. In case of X being a hadronic final state, contrary to the case of lepton pairs such as $\mu^+\mu^-$ pairs, the reconstruction of W suffers from particle losses due to a limited detector acceptance. This gives rise to the fact that the measured invariant mass W_{vis} is different from the invariant mass W. One therefore needs to unfold the true result from the visible measurement. This requires a good Monte Carlo (MC) simulation of the underlying event structure. This will be discussed in more detail in section 2.2. Only double-tagged events permit a reconstruction of W independent of the hadronic final state through the reconstruction of both photon virtualities Q^2 and P^2 from the tagged final state electrons.

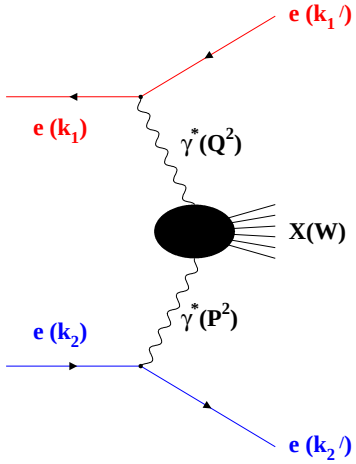

Figure 2: *Kinematics of two-photon induced processes in* e^+e^- *collisions:* k_1 *(*k_1'*)* and k_2 *(*k_2'*) are the four-momenta of the incoming (outgoing) electrons.* q *and* p *are the four-momenta of the mediated virtual photons.* W *is the invariant mass of the final state system* X.

The OPAL experiment at LEP has performed a variety of measurements of single-tagged and anti-tagged events to gain a deeper insight into the structure of the photon and its interactions. The following review will provide a summary of various measurements of those two event classes. This includes in the case of single-tagged events the investigation of the photon structure through the extraction of the photon structure function for the case of hadronic final states and a final state which consists of a $\mu^+\mu^-$ pair as well as the study of azimuthal correlations of $\mu^+\mu^-$ pairs. Anti-tagged events have been used to study the production of jets and hadrons in $\gamma\gamma$ scattering as well as for a measurement of the total hadronic $\gamma\gamma$ cross-section. Results from these measurements will be presented in

detail in section 2 for single-tagged events and section 3 for anti-tagged events. Section 4 provides a short summary and an outlook of further results on the structure of the photon and its interactions to be expected from the OPAL experiment at LEP.

2 Electron-Photon scattering

2.1 General considerations

The starting point to study eγ scattering and thus the structure of the photon in a similar way as ep scattering at LEP, is the process ee $\rightarrow$ eeX. It can be viewed as deep-inelastic scattering of an electron on a quasi-real photon. This requires to transform the cross-section $d\sigma_{\mathrm{ee}\rightarrow\mathrm{eeX}}$ into an eγ cross-section, $d\sigma_{\mathrm{e}\gamma\rightarrow\mathrm{eX}}$:

$$d\sigma_{\mathrm{ee}\rightarrow\mathrm{eeX}} = d\sigma_{\mathrm{e}\gamma\rightarrow\mathrm{eX}} \cdot f_{\gamma/\mathrm{e}} \tag{1}$$

The flux factor $f_{\gamma/\mathrm{e}}$, which denotes the flux of the target photon off the incoming electron, takes into account the momentum spread of the target photon. This is in contrast to ep scattering where the energy of both incoming particles is known. The calculation of the flux factor $f_{\gamma/\mathrm{e}}$ is carried out using the equivalent photon approximation (EPA) [4, 5]. Provided that the target photon is almost real, i.e. $P^2 \simeq 0$, and thus almost solely transversally polarized, the eγ cross-section can be reduced to two components only, σ_{TT} and σ_{LT}. The first index denotes the polarization of the probing photon whereas the second index refers to the polarization of the target photon. The following relations are defined:

$$\begin{aligned} F_1^\gamma(x,Q^2) &= \frac{Q^2}{4\pi^2\alpha}\frac{1}{2x}\cdot\sigma_{TT} \\ F_2^\gamma(x,Q^2) &= \frac{Q^2}{4\pi^2\alpha}\cdot(\sigma_{TT}+\sigma_{LT}) \end{aligned} \tag{2}$$

$F_{1,2}^\gamma$ are denoted as the photon structure functions. $F_L^\gamma = F_2^\gamma - 2xF_1^\gamma$ is the longitudinal structure function. Using these relations, the following expression for the cross-section of deep-inelastic eγ scattering is obtained:

$$\frac{d^2\sigma(\mathrm{e}\gamma\rightarrow\mathrm{eX})}{dxdQ^2} = \frac{2\pi\alpha^2}{xQ^4}\left[(1+(1-y)^2)F_2^\gamma(x,Q^2) - y^2F_L^\gamma(x,Q^2)\right] \tag{3}$$

with α being the fine structure constant. For energies of the tagged electron larger than half the beam energy, which is used to reject beam-associated background events, y is much less than 1 and thus the contribution of $y^2F_L^\gamma$ to $d^2\sigma(\mathrm{e}\gamma\rightarrow e\mathrm{X})/dxdQ^2$ is small and can therefore be neglected. In this case, $d^2\sigma(\mathrm{e}\gamma\rightarrow e\mathrm{X})/dxdQ^2$ is directly proportional to F_2^γ.

The above expression for $d^2\sigma(\mathrm{e}\gamma\rightarrow\mathrm{eX})/dxdQ^2$ is deduced for the case of transversally polarized target photons, i.e. only the two components σ_{TT} and σ_{LT} are taken into account. In case of virtual target photons ($P^2 \neq 0$), i.e. in the case of double-tagged events, this simplification no longer holds and additional cross-section terms have to be taken into account. This will change in particular the contribution of F_2^γ to $d^2\sigma(\mathrm{e}\gamma\rightarrow\mathrm{eX})/dxdQ^2$ [5, 6].

For a final state X which consists of lepton pairs (described by QED) the photon structure functions are referred to as $F_{1,2,\mathrm{QED}}^\gamma$ (leptonic structure functions), whereas for

a hadronic final state X created by a $q\bar{q}$ pair (described by QCD), the photon structure functions are denoted as $F_{1,2}^{\gamma}$ (hadronic structure functions). $F_{2,\mathrm{QED}}^{\gamma}$ is predicted by QED and a measurement of $F_{2,\mathrm{QED}}^{\gamma}$ serves as a test of QED. F_2^{γ} however cannot be calculated in a similar way from first principles for all x and Q^2. Several models have been developed based on perturbative QCD (pQCD) and a particular non-perturbative QCD ansatz. A measurement of F_2^{γ} thus allows to investigate QCD.

Despite the similarity of the differential cross-sections for $e\gamma$ scattering and ep scattering, there are subtle differences in the behavior of the structure functions which will be briefly summarized in the following.

As pointed out in the previous section, the photon shows in its interaction contributions from a point-like as well as a hadron-like behavior. The lowest-order point-like contribution, i.e. the purely electromagnetic process $\gamma^*\gamma \rightarrow q\bar{q}$, can already be predicted in the Quark-Parton model (QPM) and allows therefore a prediction of the photon structure function. The hadronic contribution cannot be calculated from first principles similarly to the case of the proton. One relies on a non-perturbative QCD input such as an estimate within the framework of the vector dominance model (VDM). F_2^{γ} is large for high values of x, whereas the proton structure function F_2^{p} decreases at large x. Furthermore, F_2^{γ} increases with Q^2 at all values of x, which is expected already from the QPM, i.e. from the point-like contribution and thus without the presence of gluon radiation. This is in striking contrast to the Q^2 dependence of F_2^{p}.

The description of the photon structure functions in terms of parton distributions and their Q^2 evolution based on the DGLAP equations can be developed in a similar way as for the proton. The point-like contribution due to the splitting process $\gamma^*\gamma \rightarrow q\bar{q}$ can be incorporated as an additional splitting function besides the usual QCD splitting functions. This additional term results in the fact that the DGLAP equations are no longer homogeneous. The solution of the inhomogeneous part is determined by the photon splitting function due to the splitting process $\gamma^*\gamma \rightarrow q\bar{q}$ whereas the homogeneous solution obeys the hadron-like evolution of the DGLAP equations.

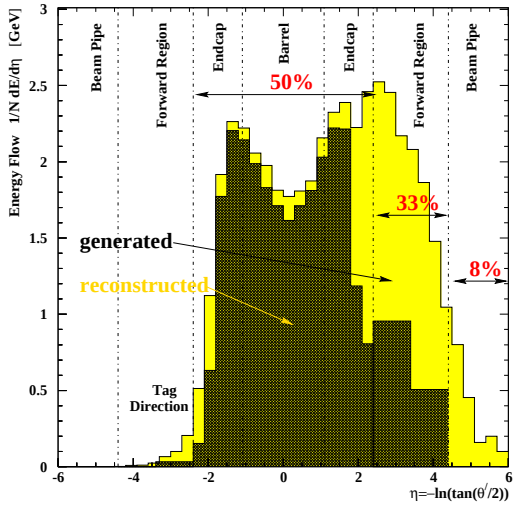

Figure 3: *Hadronic energy flow per event* $(1/N) \cdot dE/d\eta$ *as a function of pseudorapidity* η *obtained from the HERWIG MC generator.*

In summary, the hadronic photon structure function F_2^{γ} is given as the sum of a point-like, $F_2^{\gamma,\mathrm{pl}}$, and a hadron-like, $F_2^{\gamma,\mathrm{hadr.}}$, contribution:

$$F_2^{\gamma} = F_2^{\gamma,\mathrm{pl}} + F_2^{\gamma,\mathrm{hadr.}} \tag{4}$$

At large x and asymptotically large Q^2, the value of $F_2^{\gamma,\mathrm{hadr.}}$ can be calculated from pQCD. The NLO result obtained by Bardeen and Buras [7] is given as follows:

$$\frac{F_2^{\gamma}}{\alpha} = \frac{a(x)}{\alpha_s(Q^2)} + b(x) \tag{5}$$

$a(x)$ and $b(x)$ are calculable functions which diverge for $x \rightarrow 1$. $\alpha_s(Q^2)$ is the strong coupling constant. The first term reflects the LO result by Witten [8]. The Q^2 evolution

of $F_2^{\gamma,\mathrm{hadr.}}$ will eventually allow to extract the QCD scale Λ_{QCD} provided that the presence of non-perturbative contributions are under control.

Various models have been developed in the past on the description of the photon structure function such as the model by Glück, Reya and Vogt (GRV) [9] and the model by Schuler and Sjöstrand (SaS) [10]. Common to these descriptions is a non-perturbative ansatz for the hadronic contribution at a starting scale Q_0^2 and a subsequent DGLAP evolution, including a particular treatment of the charm contribution. They differ in the way this procedure is carried out. Section 2.3 will discuss in more detail these models by comparing them to experimental results on F_2^γ.

2.2 Hadronic energy flows

The measurement of the hadronic structure function F_2^γ requires the determination of the invariant mass W from the hadronic final state as pointed out in section 1. The need to unfold the invariant mass, W, from the measured result, W_{vis}, requires a modeling of the hadronic final state incorporated in a particular Monte Carlo (MC) generator. The measurement of F_2^γ and the simulation of the hadronic final state are thus closely connected.

Several investigations have been carried out by OPAL [11], comparing various observables such as the hadronic energy flow between data and MC to gain a deeper insight into the simulation of the hadronic final state. The two general purpose QCD based MC generators HERWIG [12] and PYTHIA [13] have been used for these studies. In addition, the F2GEN generator [14] has been applied to study various aspects of the simulation of a $q\bar{q}$ final state in the $\gamma^*\gamma$ centre-of-mass system. The F2GEN 'point-like' mode represents the unphysically extreme case of a two-quark state in the $\gamma^*\gamma$ centre-of-mass system with an angular distribution as in lepton pair production from two real photons. The F2GEN 'permiss' mode reflects a physics motivated mixture of point-like and peripheral interactions, where peripheral means that the transverse momentum of outgoing quarks is given by an exponential distribution as if the photons interacted as pre-existing hadrons and direct photon-quark couplings never occurred.

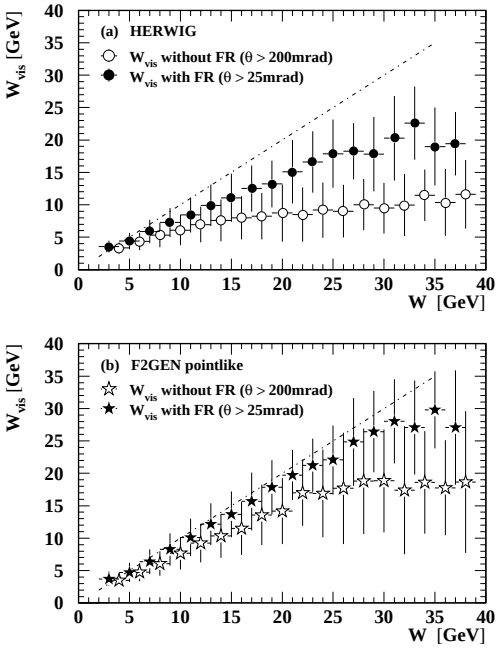

Figure 4: *Correlation between the observed hadronic invariant mass W_{vis} and the generated hadronic invariant mass W.*

The hadronic system X is strongly boosted along the beam direction, accentuating the loss of particles within the well-measured region. Figure 3 shows the prediction of the HERWIG MC generator for the hadronic energy flow per event, $(1/N) \cdot dE/d\eta$, as a function of the pseudorapidity $\eta = -\ln\tan(\theta/2)$. The tagged electron is not included in the energy flow. By definition, it lies in the negative rapidity region $-3.5 < \eta < -2.8$. The generated energy flow is shown as the light shaded region. The dark shaded region

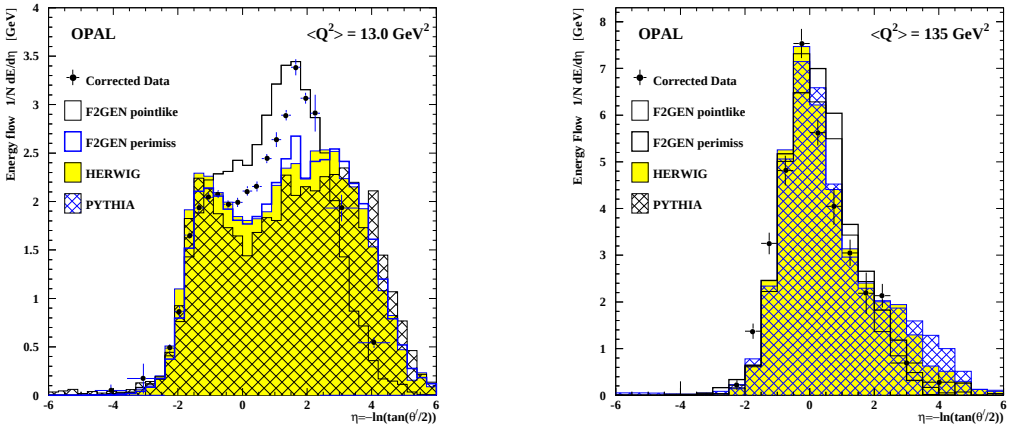

Figure 5: *Hadronic energy flow per event as a function of pseudorapidity η for low Q^2 ($Q^2 = 13.0\ GeV^2$) and high Q^2 ($Q^2 = 135\ GeV^2$) events. The data distributions have been corrected for detector effects.*

shows the energy flow after reconstruction by the OPAL detector including a simulation of the detector response. A significant fraction of the energy flow goes into the forward direction. Approximately 50% is deposited in the central region whereas 33% are deposited in the forward region. Only 8% of the total hadronic energy flow lies outside the detector acceptance. Figure 4 shows the correlation between the generated hadronic invariant mass W and the observed hadronic invariant mass $W_{\rm vis}$ with and without sampling the hadronic energy using the OPAL forward detectors (FD). Including a measurement of the hadronic energy in the forward direction by sampling the hadronic energy using the OPAL forward detectors substantially improves the correlation between W and $W_{\rm vis}$. The degree of correlation depends on the MC model.

The comparison between data and MC distributions of the hadronic energy flow is shown in Figure 5 as a function of the pseudorapidity η for two values of Q^2 of $13.0\,\mathrm{GeV}^2$ and $135\,\mathrm{GeV}^2$. The data distribution has been corrected for detector effects. Large differences are seen between data and all MC models both within the central region ($|\eta| < 2.3$), where the energy is well measured and the forward region where the energy is only sampled. The discrepancy increases towards small value of Q^2 and thus towards small values of x.

It is apparent from this section that unfolding the distribution W from the observed distribution $W_{\rm vis}$ will result in large systematic errors on the extracted photon structure function F_2^γ as long as the hadronic energy flow between the different MC models and the hadronic energy flow in data remains in clear disagreement. This is expected to affect in particular the low Q^2 and low x region.

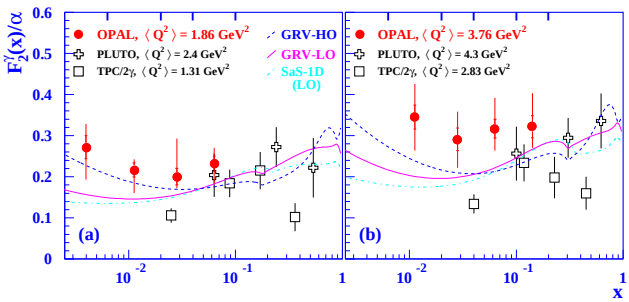

Figure 6: *OPAL results on F_2^γ/α as a function of x for $Q^2 = 1.86\,\mathrm{GeV}^2$ and $Q^2 = 3.76\,\mathrm{GeV}^2$ together with results from other experiments.*

Better general purpose MC generators are required to provide a better description of the hadronic energy flow in data and thus to reduce the large systematic uncertainties of the extracted photon structure

function F_2^γ (Section 2.3) [15]. These questions are being addressed in a LEP-wide working group with the aim of a common and consistent presentation of the hadronic energy flow in data. An improvement of general purpose MC generators based on such investigations is eagerly awaited. It is only then that an improvement in the systematic uncertainties due to the description of the hadronic final state in the extraction of F_2^γ can be expected.

2.3 Hadronic structure function F_2^γ

The measurement of the hadronic structure function F_2^γ has been carried at OPAL as a function of x and Q^2 over a wide kinematic range of $0.0025 < x \lesssim 1$ and $1.1\,\mathrm{GeV}^2 < Q^2 < 400\,\mathrm{GeV}^2$. Details on the analysis to extract F_2^γ can be found in [11,16]. The Q^2 dependence is expected to be logarithmic within the framework of pQCD. The x dependence of the proton structure function F_2^p has been studied in detail at HERA which shows a steep rise towards small values of x at not too low Q^2 values [17,18]. If the photon were purely hadron-like, a similar rise of F_2^γ is expected. A measurement of F_2^γ as a function of x and Q^2 therefore allows to shed light on the structure and the underlying dynamics of the photon as pointed out in section 2.1.

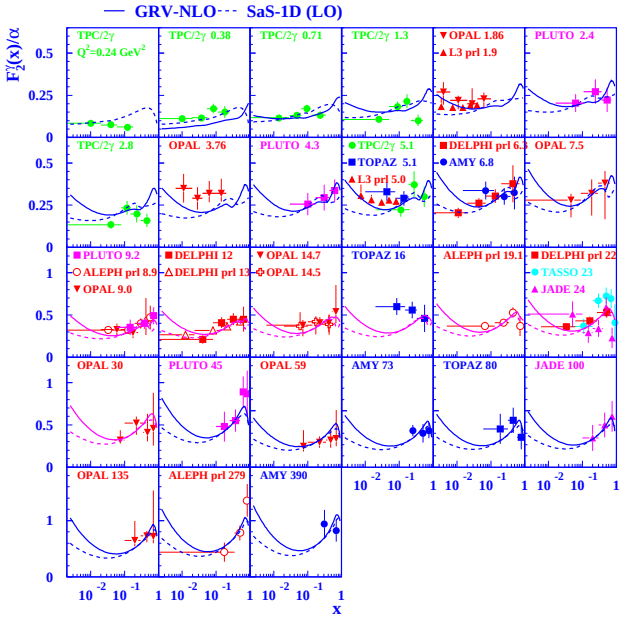

Figure 7: *OPAL results on F_2^γ/α as a function of x for several Q^2 values together with results from other experiments.*

Figure 6 shows OPAL results on F_2^γ as a function x at low values of Q^2. OPAL results on F_2^γ together with other experimental results are shown in Figure 7. The full error bars show the statistical and systematic errors added in quadrature. In Figure 6, the statistical errors are displayed by horizontal lines across the respective errors bars. The precision of the measurement is dominated by systematic uncertainties due to the modeling of the hadronic final state as pointed out in detail in the previous section. As can be seen from Figure 6, the OPAL results at the two lowest Q^2 values agree within errors with the published results from PLUTO. However, the results both from PLUTO and OPAL are higher and different in shape than the previous measurement from TPC in a similar kinematic region. Taking into account the large uncertainties, F_2^γ is found to be rather flat (Figure 6) although a small rise towards low x cannot be excluded. It can be seen from Figures 6 and 7 that F_2^γ rises smoothly towards large x. This behavior is reasonably well described by the GRV and SaS models. It can be seen from Figure 6 that the higher-order GRV prediction (GRV-HO) follows the data more closely compared to the leading-order GRV prediction (GRV-LO).

The Q^2 dependence of F_2^γ is shown in Figure 8 for the currently available data for four active flavors. It should be noted that the quoted x ranges by different experiments are not the same which makes a comparison rather difficult since several predictions for different ranges in x show a large difference for $Q^2 > 100\,\mathrm{GeV}^2$. All results on F_2^γ as shown in Figure 8 agree reasonably well, taking into account the large uncertainties. A

logarithmic rise of F_2^γ is seen in the data as predicted by pQCD. However, the systematic uncertainties on F_2^γ are too large to perform a precision test of pQCD. Both, the GRV and SaS model allow to describe the data equally well. The observed logarithmic rise of F_2^γ in Q^2 can be reasonably well represented by the pQCD leading order asymptotic solution. It is found that the hadronic contribution to F_2^γ decreases towards larger x and Q^2 values, and amounts to only about 15% at $Q^2 = 59\,\mathrm{GeV}^2$ and $x = 0.5$.

All OPAL results on F_2^γ have not been corrected for the fact that in the single-tagged mode, P^2 is only approximately zero. Several theoretical predictions exit on how F_2^γ varies as a function of P^2 [19]. It has been estimated based on the SaS model that F_2^γ with $P^2 \neq 0$ would be approximately 10% lower compared to the case of $P^2 = 0$. The P^2 distribution in the data and the correct theoretical prescription are not known. This is reason why no correction has been applied to the data on F_2^γ. The larger centre-of-mass energy at LEP compared to former experiments at PETRA makes this effect to become more important. The investigation of the virtual structure of the photon through double-tag events and the measurement of $F_{2,\mathrm{QED}}^\gamma$ (Section 2.4) will allow to gain some experimental knowledge in that respect.

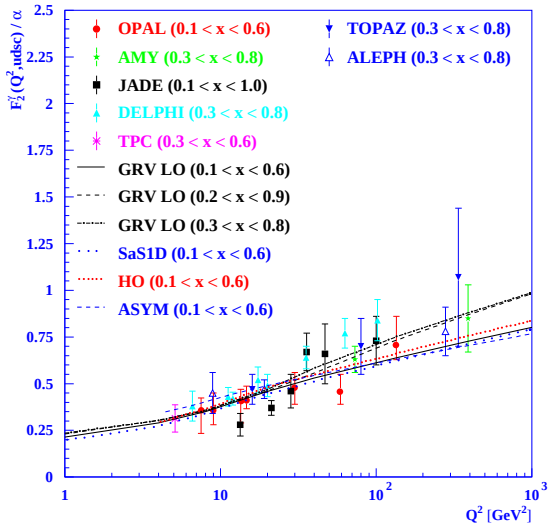

Figure 8: *OPAL results on F_2^γ/α as a function of Q^2 for different ranges in x together with results from other experiments [20].*

Improvements in the precision of F_2^γ require considerable improvements of general purpose MC models to better describe the hadronic final state. It is only then that the study of the low x behavior of F_2^γ as well as as the Q^2 evolution could be carried out with higher precision.

2.4 Leptonic structure function $F_{2,\mathrm{QED}}^\gamma$

The differential cross-section (3) with $\gamma^*\gamma \to \mathrm{l}^+\mathrm{l}^-$ allows to measure the leptonic structure function of the photon, $F_{2,\mathrm{QED}}^\gamma$. A measurement of $F_{2,\mathrm{QED}}^\gamma$ has been carried out at OPAL by reconstructing $\mu^+\mu^-$ pairs in the final state [21]. Such a clean environment allows to unfold the invariant mass W from the observed invariant mass W_{vis} with higher precision compared to the case of a hadronic final state which yields a much more precise determination of the leptonic photon structure function compared to the hadronic case.

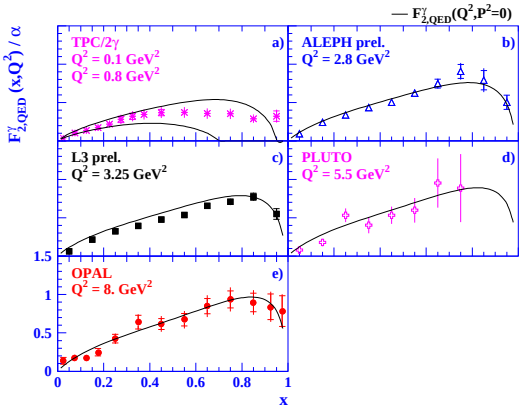

Figure 9: $F_{2,\mathrm{QED}}^\gamma/\alpha$ *as a function of x [20].*

Figure 9 shows OPAL results on $F_{2,\mathrm{QED}}^\gamma$ as a function of x together with other experiments. The full error bars show the statistical and systematic errors added in quadrature,

whereas the statistical errors are displayed by horizontal lines across the respective errors bars. The precision of the data allow for a test of QED. The solid lines in Figure 9 show the results of a QED calculation. All measurements are consistent with QED expectations. The data are so precise that subtle effects such as the P^2 dependence can be investigated in more detail.

2.5 Azimuthal correlations of lepton pairs

It has been pointed out that azimuthal correlations in the final-state particles of two photon collisions, i.e. $\gamma^*\gamma \to$ X, are sensitive to additional structure functions [22]. Azimuthal correlations can therefore supplement the direct measurement of the photon structure functions.

OPAL has performed a measurement of azimuthal correlations in single-tagged events of $\gamma^*\gamma \to \mu^+\mu^-$ [23]. Two angles are defined which allow azimuthal correlations and thus more subtle structure functions to be studied. The azimuthal angle χ is the angle between the planes defined by the $\gamma^*\gamma$ axis and the two-body final state and the $\gamma^*\gamma$ axis and the tagged electron. The second angle $\eta = \cos\theta^*$ is defined by the angle θ^* as the angle between the μ^- and the $\gamma^*\gamma$ axis.

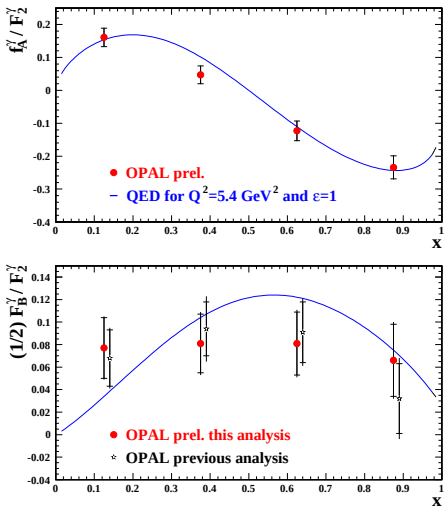

Figure 10: *OPAL results on the ratios* f_A^γ/F_2^γ *and* $(1/2)F_B^\gamma/F_2^\gamma$ *as a function of* x.

With the assumption that the target photon is only transversely polarized, the cross-section for $e\gamma \to e\mu^+\mu^-$ differential in x, y and the two angles χ and η is given as follows:

$$\frac{d\sigma(e\gamma \to e\mu^+\mu^-)}{dxdyd\eta d\chi/2\pi} \approx \frac{2\pi\alpha^2}{Q^2}\left(\frac{1+(1-y)^2}{xy}\right)\left[2x\tilde{F}_T^\gamma + \tilde{F}_L^\gamma - \tilde{F}_A^\gamma\cos\chi + \frac{\tilde{F}_B^\gamma}{2}\cos 2\chi\right] \quad (6)$$

The conventional structure functions can be recovered by integrating over χ and η:

$$F_{T,L,A,B}^\gamma = \frac{1}{2\pi}\int_{-1}^{+1} d\eta \int_0^{2\pi} d\chi \tilde{F}_{T,L,A,B}^\gamma \quad (7)$$

In leading order and for massless muons, the following identity holds, $F_B^\gamma = F_L^\gamma$ although F_B^γ and F_L^γ are due to different helicity states of the photon. The structure function F_A^γ results from interference terms between longitudinal and transverse photons whereas the structure function F_B^γ refers to interference terms between solely transverse polarized photons. Figure 10 shows published and preliminary results on the x dependence of the ratios f_A^γ/F_2^γ and $(1/2)F_B^\gamma/F_2^\gamma$ where $f_A^\gamma = (1/2)(f_A^+ - f_A^-)$ with $f_A^+ = (1/2\pi)\int_0^{+1} d\eta \int_0^{2\pi} d\chi \tilde{F}_A^\gamma$ and $f_A^- = (1/2\pi)\int_{-1}^{0} d\eta \int_0^{2\pi} d\chi \tilde{F}_A^\gamma$. The solid line is the result of a QED prediction. The observed variation in x of the data is consistent with QED. Both ratios are significantly different from zero. These results not only serve as an interesting approach to supplement the conventional structure function measurements in itself, they also mark the first step to perform such a measurement in the much more complex environment of a hadronic final state.

3 Photon-Photon scattering

3.1 Introduction

Anti-tagged events in e^+e^- scattering at LEP allow to study collisions of two quasi-real photons, i.e. $\gamma\gamma \to X$ with $Q^2 \simeq 0$ and $P^2 \simeq 0$ as introduced in section 1. The median Q^2 (P^2) amounts to approximately $10^{-4}\,\mathrm{GeV}^2$ for $Q^2 < 4\,\mathrm{GeV}^2$. The e^+e^- collider LEP is in this respect a $\gamma\gamma$ collider with a centre-of-mass energy of the $\gamma\gamma$ system of $10 < W_{\gamma\gamma} < 110\,\mathrm{GeV}$.

The interaction of two photons can be classified to be either a direct process where two bare photons interact, a single-resolved process where a bare photon interacts with a parton of the other photon or a double-resolved process where partons of both photons interact together. The last two processes are due to the possibility of a photon to interact as a hadronic fluctuation. This classification is only uniquely defined in LO QCD, but not in NLO QCD.

In LO QCD, the experimental signature, neglecting multiple parton interactions, consists of two hard parton jets with large transverse energy E_T^{jet} (direct events). In single- or double-resolved interactions, the two hard parton jets are expected to be accompanied by one or two remnant jets.

The cone jet finding algorithm has been applied throughout the following studies unless otherwise specified.

The above three event classes can be separated using the fraction of the photon's momentum which participates in the hard interaction. It can be specified using the following relations [22]:

$$x_\gamma^{\pm} = \frac{\sum_{\mathrm{jets}=1,2}(E \pm p_z)}{\sum_{\mathrm{hadrons}}(E \pm p_z)} \qquad (8)$$

p_z is the momentum component along the z axis and E is the energy of the respective energy depositions of the jets or hadrons. These variables provide some separation of direct and resolved two-jet events [24]

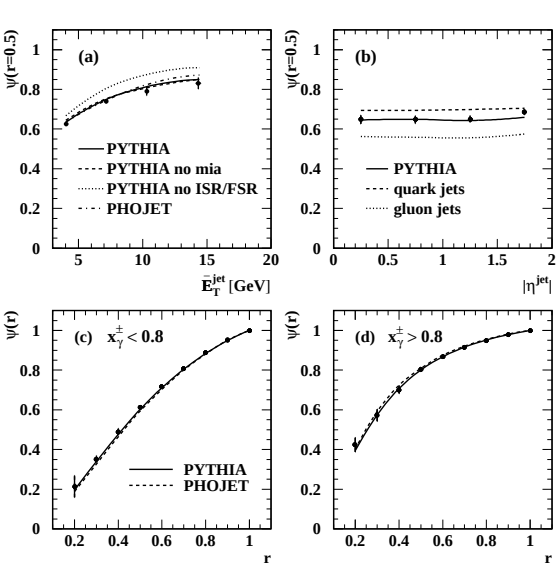

Figure 11: *Jet shape $\psi(r = 0.5)$ as a function of $\bar{E}_T^{\mathrm{jet}}$ (a) and $|\eta^{\mathrm{jet}}|$ (b). $\psi(r)$ as a function of r for $x_\gamma^{\pm} < 0.8$ (c) and $x_\gamma^{\pm} > 0.8$ (d).*

The underlying processes for $\gamma\gamma$ scattering have been calculated in LO [25] and NLO perturbative QCD (pQCD) [26]. In the case of direct events, the only LO contributing matrix element is $\gamma\gamma \to q\bar{q}$ whereas for double-resolved events, quark-gluon, gluon-quark and gluon-gluon type matrix elements have to be taken into account. The observed jet events are thus related to the underlying dynamics which allows to examine the structure the photon and the dynamics of the $\gamma\gamma$ processes. The measured inclusive two-jet cross-section as well as the angular distribution of the parton scattering angle in the two-jet centre-of-mass frame have been compared to NLO pQCD calculations. These two items together with a study of jet shapes in two-jet events and an investigation of the influence of an underlying event in two-jet events will be presented

in the next section. The production of charged hadrons and χ_{c2} mesons will be discussed in section 3.3. The measurement of the total hadronic $\gamma\gamma$ cross-section will be focused on in detail in section 3.4.

3.2 Jet production

3.2.1 Jet shapes

The internal structure of jets produced in two-jet events has been studied based on the following jet shape definition:

$$\psi(r) = \frac{1}{N_{\rm jet}} \sum_{\rm jet} \frac{E_T(r)}{E_T(r=R)} \qquad (9)$$

$\psi(r)$ denotes the fraction of the jet's energy that lies inside an inner cone of radius r, thus $\psi(r=R)=1$. $E_T(r)$ is the transverse energy within the inner cone of radius r and $N_{\rm jet}$ refers to the total number of jets in the sample.

Figure 11 shows the fraction of the transverse energy of the jets inside a cone of radius $r=0.5$ around the jet axis (a) as a function of $\bar{E}_T = (1/2)(E_T^{\rm jet1}+E_T^{\rm jet2})$ and (b) as a function of $|\eta^{\rm jet}| = |(1/2)(\eta^{\rm jet1} + \eta^{\rm jet2})|$ with $E_T^{{\rm jet}\,i}$ and $\eta^{{\rm jet}\,i}$ defined in the lab frame. The jet shapes have been corrected to the hadron level. The data points are compared to PYTHIA with and without multiple interactions and to PYTHIA with and without initial (ISR) and final state (FSR) QCD radiation along with a prediction from PHOJET [27]. Jets without initial and final state QCD radiation are significantly narrower. Multiple interactions as simulated within PYTHIA have only a minor effect on the jet shape. As expected, the jets become narrower with increasing $\bar{E}_T$. No significant dependence of $\psi(r=0.5)$ on $|\eta^{\rm jet}|$ has been found.

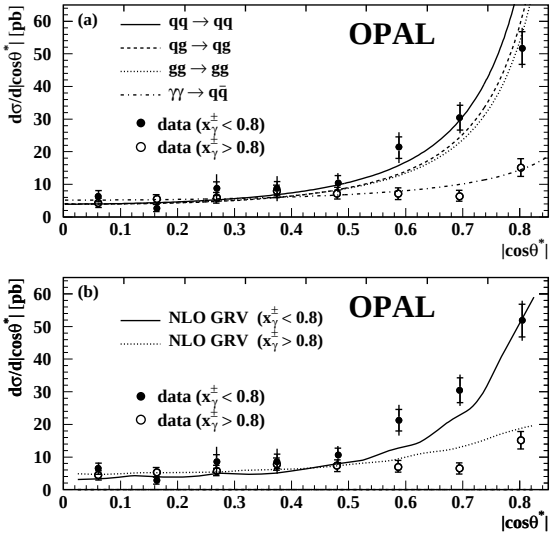

Figure 12: *Angular distribution* $d\sigma/d|\cos\theta^*|$ *as function of* $|\cos\theta^*|$ *for* $x_\gamma^\pm > 0.8$ *and* $x_\gamma^\pm < 0.8$ *in comparison to NLO pQCD calculations.*

The gluon and quark content in direct and double-resolved events is expected to be different from the above discussion in section 3.1. Samples of large fractions of direct and double-resolved events have been selected by requiring $x_\gamma^\pm$ to be larger or less than 0.8, respectively. The jet shape $\psi(r)$ is shown in Figure 11 as a function of r for $x_\gamma^\pm < 0.8$ (c) and $x_\gamma^\pm > 0.8$ (d). The observed jet shapes are found to be broader for the double-resolved event sample ($x_\gamma^\pm < 0.8$) than those for direct events ($x_\gamma^\pm > 0.8$). Gluon jets are known to be broader than quark jets which is consistent with the difference in the jet shapes of direct and double-resolved events due to the expected difference in the gluon and quark composition.

The PYTHIA and PHOJET jet shape prediction are found to be in good agreement with the data.

3.2.2 Angular distributions in direct and resolved events

The angular distribution for direct and double-resolved events in the two-jet centre-of-mass frame is expected to be different due to the different gluon and quark composition

and thus the different contributing matrix elements. The angle $\cos\theta^*$ between the jet axis and the axis of the incoming partons or direct photons in the two-jet centre-of-mass frame can be estimated as follows:

$$\cos\theta^* = \tanh\left(\frac{\eta^{\mathrm{jet1}} - \eta^{\mathrm{jet2}}}{2}\right) \tag{10}$$

In LO, the direct process $\gamma\gamma \to \mathrm{q\bar{q}}$ leads to an angular dependence of the form $\propto 1/(1-\cos^2\theta^*)$ whereas for double-resolved events which involves gluon initiated matrix elements, the angular dependence can be approximated as $\propto 1/(1-\cos^2\theta^*)^2$.

Figure 12 shows the angular distribution $d\sigma/d|\cos\theta^*|$ as a function of $|\cos\theta^*|$ for samples with a large fraction of direct ($x_\gamma^\pm > 0.8$) and double-resolved ($x_\gamma^\pm < 0.8$) events. The data are compared to NLO pQCD calculations for the cross-section $d\sigma/d|\cos\theta^*|$ and the contributing single cross-sections. Events with $x_\gamma^\pm > 0.8$ show only a small rise with increasing $|\cos\theta^*|$ whereas events with $x_\gamma^\pm < 0.8$ show a much larger rise as a function of $|\cos\theta^*|$. This behavior follows the QCD expectation taking into account the expected difference in the gluon and quark composition of direct and double-resolved events. The result of the NLO pQCD calculations agrees well with the observed shape of the data.

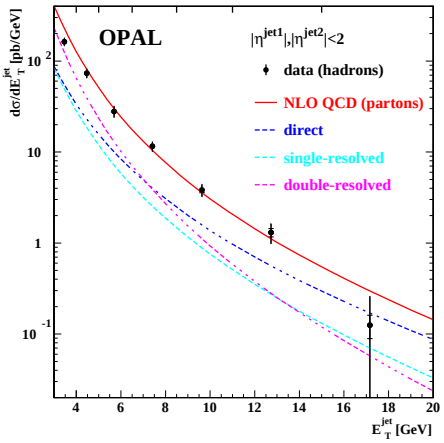

Figure 13: *The inclusive two-jet cross-section as a function of E_T^{jet} for $|\eta^{\mathrm{jet}}| < 2$ in comparison to NLO pQCD calculations.*

3.2.3 Inclusive two-jet cross-section and NLO calculations

Figure 14 shows the inclusive two-jet cross-section as a function of E_T^{jet} for $|\eta^{\mathrm{jet}}| < 2$ at $\sqrt{s_{\mathrm{e^+e^-}}} = 161 - 172\,\mathrm{GeV}$. The measurements are compared to NLO pQCD calculations by Kleinwort and Kramer [28] which are using the GRV parton parameterizations of the photon. The predictions for the direct, single- and double-resolved contributions as well as their sum are shown separately. The data points are in good agreement with NLO pQCD calculations except for the first bin. However, experimental as well as theoretical uncertainties are large in this kinematic region. The direct component dominates the cross-section at high E_T^{jet}, whereas the resolved cross-section is the largest component for $E_T^{\mathrm{jet}} < 8\,\mathrm{GeV}$.

3.2.4 Influence of the underlying event

The possibility for an underlying event in the $\gamma\gamma$ scattering process is not taken into account in the NLO pQCD calculations. However, an underlying event leads to an increased jet cross-section. Resolved photons such as in double-resolved events involve multiple partons which are subject to multiple interactions. The effect of the simulation of the underlying event is therefore important. The MC models PYTHIA and PHOJET use the concept of multiple interactions in the simulation of the underlying event. The contribution of multiple interactions has to be tuned using quantities which are not directly correlated to the jets. Only then effects due to parton distributions and due to the

underlying event can be disentangled. The model dependence for the simulation of the underlying event through multiple interactions can be tuned using the transverse cutoff parameter $p_t^{\rm mi}$ for multiple interactions.

The investigation of an underlying event in the $\gamma\gamma$ scattering process starts from the observation that the transverse energy flow outside the jets measured as a function of x_γ is correlated to the underlying event [29]. At small x_γ, the transverse energy flow outside the jets increases which can be used to tune the number of multiple interactions. The transverse energy flow corrected to the hadron level outside the jets, excluding the region of $R < 1.3$ in the energy sum, is shown in Figure 14 as a function of x_γ in comparison to different MC model predictions using different values for $p_t^{\rm mi}$. The impact of multiple interactions has been found to be large for PYTHIA and PHOJET using the LAC1 parameterization. Their impact is small when using either GRV or SaS-1D. The optimal transverse cutoff parameter $p_t^{\rm mi}$ shows a strong dependence on the underlying parton distributions in case of PYTHIA. Using GRV, $p_t^{\rm mi}$ has been set to 2.0 GeV, SaS-1D requires a value for $p_t^{\rm mi}$ of 1.4 GeV whereas for LAC1, $p_t^{\rm mi}$ has been set to 2.5 GeV. In case of PHOJET the default cutoff parameter $p_t^{\rm mi}$ of 2.5 GeV provides for GRV as well as for SaS-1D a reasonable description of the transverse energy flow.

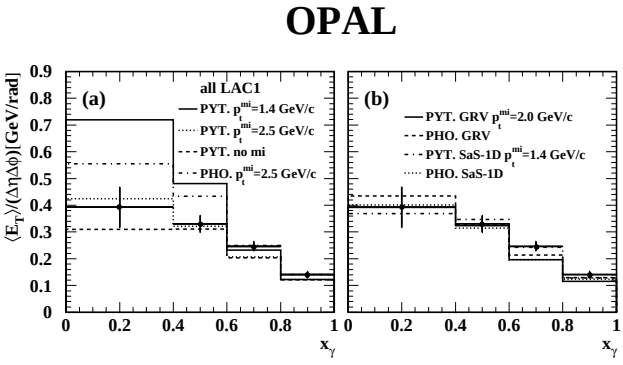

Figure 14: *Transverse energy flow outside the jets in the central rapidity region* $|\eta^*| < 1$ *as a function of* x_γ.

3.2.5 Inclusive two-jet cross-section as a function of $|\eta^{\rm jet}|$

Having tuned the simulation of the underlying event through multiple interactions using the transverse cutoff parameter $p_t^{\rm mi}$, the sensitivity of the jet cross-section on the underlying parton distribution can be investigated. The inclusive two-jet cross-section is shown in Figure 15 as a function of $|\eta^{\rm jet}|$ for $E_T^{\rm jet1} > 5\,$GeV and $E_T^{\rm jet2} > 3\,$GeV with (left) large samples of double-resolved events ($x_\gamma^\pm < 0.8$) and (right) large samples of direct events ($x_\gamma^\pm > 0.8$). A large dependence on the underlying parton distribution is found for double-resolved events compared to direct events. The impact of the gluon distribution is expected to be larger for double-resolved events compared to direct events. LAC1 compared to GRV and SaS-1D, which increases the cross-section for gluon-initiated processes, leads to a strong overestimation of the two-jet cross-section.

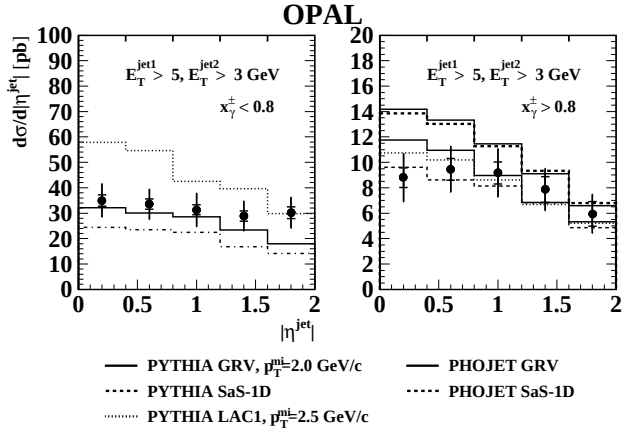

Figure 15: *Inclusive two-jet cross-section as a function of* $|\eta^{\rm jet}|$ *for (left)* $x_\gamma^\pm < 0.8$ *and (right)* $x_\gamma^\pm > 0.8$.

3.3 Hadron production

3.3.1 Production of charged hadrons

The contribution of direct photon processes in photon induced interactions is expected to lead to a harder transverse momentum distribution of charged hadrons for $\gamma\gamma$ scattering than for γp or hadron-p scattering. The p_T distribution for $\gamma\gamma$ scattering as obtained by OPAL [30] with $10 < W < 30\,\text{GeV}$ is shown in Figure 16 together with data on γp, πp and Kp data from WA69 with a hadronic invariant mass of 16 GeV. The WA69 data are normalized to the $\gamma\gamma$ data at $p_T \approx 200\,\text{MeV}$. ZEUS data on charged particle production in γp scattering with a diffractively dissociated photon, having an average invariant mass of the 'γ-Pomeron' system of 10 GeV, are shown as well.

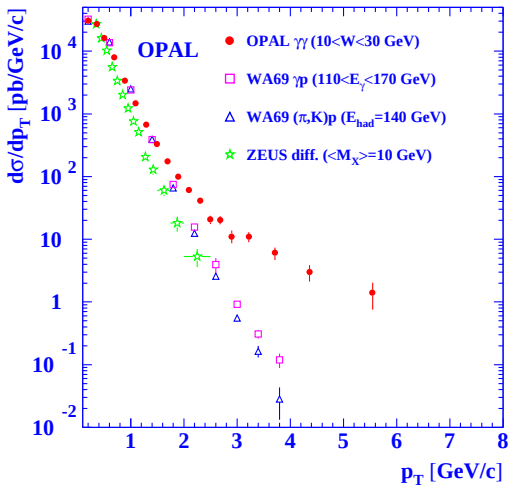

Figure 16: *p_T distribution of $\gamma\gamma$, γp, πp and* Kp *scattering.*

It can be clearly inferred from Figure 16 that $\gamma\gamma$ interactions show a significantly harder p_T distribution than γp and hadron-p interactions. The measured p_T distribution has been compared to NLO pQCD calculations which have been found to be in good agreement with the data. The direct interactions yield the largest contribution at high p_T compared to single- and double-resolved interactions.

3.3.2 Production of χ_{c2} mesons

OPAL has carried out an analysis reconstructing χ_{c2} mesons in the decay channel $\chi_{c2} \to J/\psi\ \gamma \to \text{l}^+\text{l}^-\gamma \quad (\text{l} = \text{e}, \mu)$ which resulted in a measurement of the two-photon width $\Gamma(\chi_{c2} \to \gamma\gamma)$ [31]. The data sample consists of all data taken at e^+e^- centre-of-mass energies of 91 GeV and 183 GeV corresponding to integrated luminosities of $167\,\text{pb}^{-1}$ and $55\,\text{pb}^{-1}$, respectively. Figure 17 shows the mass difference between the llγ and ll invariant masses, $M_{\text{ll}\gamma} - M_{\text{ll}}$. 34 events have been selected in the χ_{c2} signal region of $330 < M_{\text{ll}\gamma} - M_{\text{ll}} < 550\,\text{MeV}$ including a background of 12.4 ± 3.3 events. The contribution from χ_{c0} and χ_{c1} is estimated not to exceed a few percent. The two-photon width has been determined to be $\Gamma(\chi_{c2} \to \gamma\gamma) = 1.76 \pm 0.47 \pm 0.37 \pm 0.15\,\text{keV}$. The first error denotes the statistical and the second the systematic error. The third error reflects the uncertainty of the branching ratios in the decay $\chi_{c2} \to J/\psi\ \gamma \to \text{l}^+\text{l}^-\gamma$. This

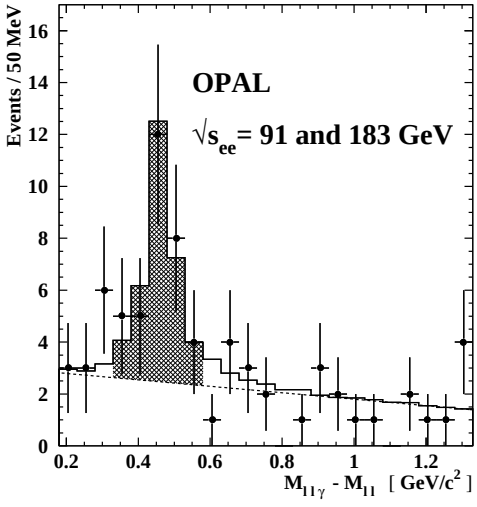

Figure 17: *Mass difference between the* llγ *and* ll *invariant masses, $M_{\text{ll}\gamma} - M_{\text{ll}}$.*

result agrees with results from CLEO, TPC/2γ and R704, but is about two standard deviations larger than the E760 result and the current world average [32]. Furthermore the determined two-photon width is found to be two standard deviations larger than the prediction by Schuler [33].

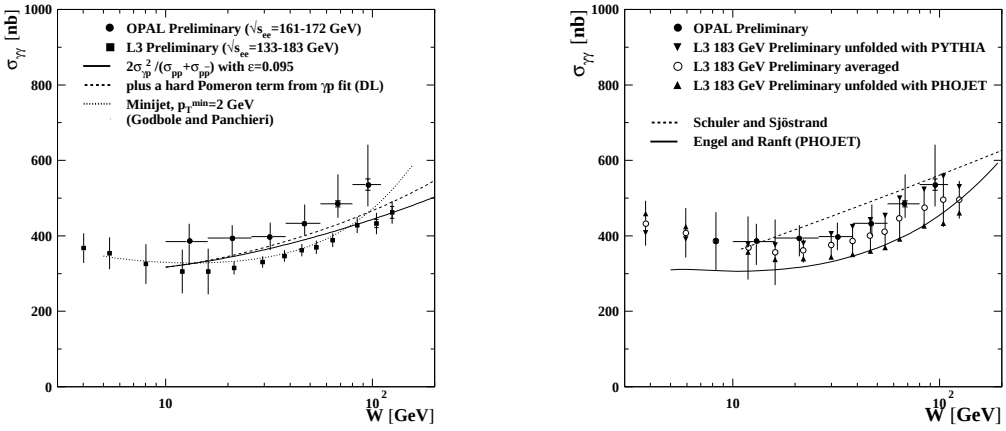

Figure 18: *Total cross-section for $\gamma\gamma \rightarrow$ hadrons, $\sigma_{\gamma\gamma}$, as a function of $W = \sqrt{s_{\gamma\gamma}}$ from OPAL in comparison to L3 results and theoretical predictions (left). Comparison of preliminary OPAL results on $\sigma_{\gamma\gamma}$ with L3 results obtained with PYTHIA and PHOJET (right) [34].*

3.4 Total cross-sections

The total cross-section for $\gamma\gamma \rightarrow$ hadrons, $\sigma_{\gamma\gamma}$, at large centre-of-mass energies $W = \sqrt{s_{\gamma\gamma}}$ is expected to be dominated by interactions of hadronic fluctuations of the colliding photons. A measurement of $\sigma_{\gamma\gamma}$ should therefore improve our understanding of the hadronic nature of the photon and in particular clarify the question whether the W dependence of $\sigma_{\gamma\gamma}$ exhibits the same behavior as total hadronic cross-sections. This could lead to an answer of the question if there is an universal behavior of total cross-sections in $\gamma\gamma$, γp and pp/p$\bar{\text{p}}$ scattering.

Pre-Lep data are restricted to rather low energies in W, which is too low to observe the expected rise of total hadronic cross-sections due to Pomeron exchange in the language of Regge phenomenology. A measurement at LEP taking into account the large centre-of-mass energy compared to previous experiments at PETRA allow to study the behavior of $\sigma_{\gamma\gamma}$ at higher energies.

The extraction of the total cross-section, $\sigma_{\gamma\gamma}$, relies heavily on a particular Monte Carlo (MC) program to be used for the unfolding. It is therefore expected that systematic uncertainties on the extracted total cross-sections are dominated by the simulation of the hadronic final state.

Figure 18 (left) shows the preliminary OPAL results [35] on the total cross-section, $\sigma_{\gamma\gamma}$, as a function of $W = \sqrt{s_{\gamma\gamma}}$ in the range of $10 \leq W \leq 110\,\text{GeV}$ in comparison to L3 results [36] for $5 \leq W \leq 145\,\text{GeV}$. Various curves from theoretical predictions are overlaid. The preliminary OPAL cross-section results are quoted by taking the average of the cross-section results obtained with the MC models PHOJET and PYTHIA. The difference between theses results has been included in the systematic error evaluation. However, L3 has used PHOJET to determine the central values. No model dependence is reflected in

their quoted systematic errors. The unfolded L3 results using PHOJET and PYTHIA together with their average values are shown in Figure 18 (right). Comparing theses cross-section values with the preliminary results obtained by OPAL and thus providing a consistent bases for a detailed comparison, no significant discrepancy between both results is found.

Relating the total cross-section, $\sigma_{\gamma\gamma}$, to the total cross-sections for γp, pp and $\bar{\text{p}}$p scattering, results in the prediction shown as the solid line in Figure 18 (left). It describes the general trend of $\sigma_{\gamma\gamma}$ as a function of W. It has been argued by many authors to expect a faster rise of the total cross-section for $\gamma\gamma$ scattering compared to γp scattering and hadron-hadron scattering due to the possibility of two photons interacting directly. In a Regge-type fit to the data, L3 determined a Pomeron intercept of $\alpha_{I\!P} = 1.158 \pm 0.006\,(\text{stat}) \pm 0.028\,(\text{sys})$ which is larger than the Pomeron intercept of $\alpha_{I\!P} = 1.100 \pm 0.002\,(\text{stat}) \pm 0.012\,(\text{sys})$ obtained from a recent ZEUS analysis of total γp cross-section results based on an extrapolation of total γ^*p cross-section data [17]. The soft Pomeron intercept by Donnachie and Landshoff [37] of $\alpha_{I\!P} = 1.0808$ is smaller than those obtained from total-cross section results involving at least one photon in the scattering process.

4 Summary and Outlook

OPAL has performed a wide range of measurements of eγ and $\gamma\gamma$ scattering in e^+e^- collisions at LEP.

The hadronic photon structure function F_2^γ has been measured for $0.0025 < x \lesssim 1$ and $1.1 < Q^2 < 400\,\text{GeV}^2$. The current systematic uncertainties on F_2^γ are dominated by the model dependence in the simulation of the hadronic final state. Only considerable improvements of general purpose Monte Carlo (MC) models to better describe the hadronic final state will allow to study the low x behavior of F_2^γ as well as the Q^2 evolution with higher precision. Data on the leptonic structure function $F_{2,\text{QED}}^\gamma$ are precise enough to test QED and to be sensitive to more subtle effects such as the P^2 dependence.

It has been shown that the measured inclusive two-jet cross-sections in $\gamma\gamma$ scattering can be well understood within the framework of NLO perturbative QCD (pQCD). Two-jet cross-section measurements provide a useful means to constrain the gluon density in the photon. The total cross-section results of the process $\gamma\gamma \to$ hadrons from OPAL and L3 were shown to be consistent. It has been found that the total $\gamma\gamma$ cross-section rises faster with W than in γp scattering and even faster than in pp or p$\bar{\text{p}}$ scattering.

The main concern for future measurements of F_2^γ and $\sigma_{\gamma\gamma}$ is to reduce the large systematic uncertainties due to the simulation of the hadronic final state. Improvements of general purpose MC models are eagerly awaited [15]. With the larger centre-of-mass energy $\sqrt{s_{\text{e}^+\text{e}^-}}$ at LEP2 and the higher statistics it will be possible to extend the kinematic range towards larger values in Q^2 and W^2. Finally, the study of double-tagged events to investigate the virtual structure of the photon will be one of the main analysis topics for the future.

An exciting time is ahead of us until 2000 investigating the structure of the photon and its interactions at LEP2[2].

[2] At the time of writing this report, the OPAL experiment at LEP has recorded more than $175\,\text{pb}^{-1}$ of data during the '98 run at a centre-of-mass energy of 189 GeV.

Acknowledgement

I want to thank Richard Nisius, Gerhard Schuler and Stefan Söldner-Rembold for carefully reading the manuscript. I am very grateful to Goran Jarlskog for giving me the opportunity to go to this excellent workshop.

References

[1] B.L. Ioffe, *Phys. Lett.* **B 30** (1969) 123.

[2] J.J. Sakurai, *Ann. Phys.* **11** (1960) 1.

[3] M. Erdmann, talk given at the XXIX International Conference on High Energy Physics, Vancouver, Canada, July 1998.

[4] C.F. von Weizsäcker, *Z. Phys.* **88** (1934) 612;
E.J. Williams, *Phys. Rev.* **45** (1934) 729;
P. Kessler, Il Nuovo Cimento **17** (1960) 809.

[5] V.M. Budnev *et al.*, *Phys. Rep.* **15** (1975) 181.

[6] PLUTO Collaboration, C. Berger *et al.*, *Phys. Lett.* **B 142** (1984) 119;
C. Berger and W. Wagner, *Phys. Rep.* **146** (1987) 1;
M. Stratmann, these proceedings.

[7] W.A. Bardeen and A.J. Buras, *Phys. Rev.* **D20** (1979) 166;
W.A. Bardeen and A.J. Buras, *Phys. Rev.* **D21** (1980) 2041.

[8] E. Witten, *Nucl. Phys.* **B104** (1976) 445.

[9] M. Glück *et al.*, *Phys. Rev.* **D46** (1992) 1973;
M. Glück *et al.*, *Phys. Rev.* **D45** (1992) 3986.

[10] G.A. Schuler and T. Sjöstrand, *Z. Phys.* **C68** (1995) 607.

[11] OPAL Collaboration, K. Ackerstaff *et al.*, Z. Phys. **C74** (1997) 33.

[12] G. Marchesini and B.R. Webber, Nucl. Phys. **B238** (1984) 1.

[13] T. Sjöstrand, Comp. Phys. Comm. **82** (1994) 74.

[14] A. Buijs, W.G.J. Langeveld, M.H. Lehto and D.J. Miller, Comp. Phys. Comm. **79** (1994) 523.

[15] Leif Lönnblad, these proceedings.

[16] OPAL Collaboration, K. Ackerstaff *et al.*, Phys. Lett. **B412** (1997) 225;
OPAL Collaboration, K. Ackerstaff *et al.*, Phys. Lett. **B411** (1997) 387.

[17] ZEUS Collaboration, J. Breitweg *et al.*, DESY-98-121.

[18] H1 Collaboration, C. Adloff *et al.*, Nucl. Phys. **B497** (1997) 3;
ZEUS Collaboration, J. Breitweg *et al.*, Phys. Lett. **B407** (1997) 432;
ZEUS Collaboration, M. Derrick *et al.*, Z. Phys. **C72** (1996) 399.

[19] G.A. Schuler and T. Sjöstrand, *Phys. Lett.* **B376** (1996) 193;
M. Glück *et al.*, *Phys. Rev.* **D54** (1996) 5515;
M. Glück *et al.*, *Phys. Rev.* **D51** (1995) 3220;
M. Dress and R.M. Godbole, *Phys. Rev.* **D50** (1994) 3124.

[20] R. Nisius, talk given at the International Europhysics Conference on High Energy Physics, Jerusalem, Israel, August 1997, hep-ex/9712012.

[21] OPAL Collaboration, R. Akers *et al.*, Z. Phys. **C60** (1993) 593.

[22] P. Aurenche *et al.*, in *Proceedings of the Workshop on Physics at LEP2*, edited by G. Altarelli, T. Sjöstrand and F. Zwirner (Geneva, Switzerland, 1996), CERN 96-01.

[23] OPAL Collaboration, K. Ackerstaff *et al.*, Z. Phys. **C74** (1997) 49.
K. Freudenreich, talk given at the XXIX International Conference on High Energy Physics, Vancouver, Canada, July 1998.

[24] OPAL Collaboration, K. Ackerstaff *et al.*, Z. Phys. **C73** (1997) 433.

[25] D.W. Duke and J.F. Owens, Phys. Rev. **D26** (1982) 1600;
B.L. Combridge *et al.*, Phys. Lett. **B70** (1977) 234.

[26] M. Klasen, T. Kleinwort and G. Kramer, Eur. Phys. J. direct, **C1** (1998) 1.

[27] R. Engel, Z. Phys. **C66** (1995) 203;
R. Engel and J. Ranft, Phys. Rev. **D54** (1996) 4246.

[28] T. Kleinwort and G. Kramer, Nucl. Phys. **B477** (1996) 3;
T. Kleinwort and G. Kramer, Phys. Lett. **370** (1996) 141.

[29] H1 Collaboration, S. Aid *et al.*, Z. Phys. **C70** (1996) 17.

[30] OPAL Collaboration, K. Ackerstaff *et al.*, CERN-EP/98-091.

[31] OPAL Collaboration, K. Ackerstaff *et al.*, CERN-EP/98-106.

[32] Particle Data Group, Review of Particle Physics, Eur. Phys. J. **C3** (1998) 1.

[33] G.A. Schuler, F.A. Berends and R. van Gulik, Nucl. Phys. **B523** (1998) 423.

[34] S. Söldner-Rembold, talk given at the 18th International Symposium on Lepton - Photon Interactions, Hamburg, Germany, August 1997, hep-ex/9711005.

[35] OPAL Collaboration, paper 199 submitted to the XXIX International Conference on High Energy Physics, Vancouver, Canada, July 1998.

[36] L3 Collaboration, M. Acciarri *et al.*, Phys. Lett. **B408** (1997) 450.

[37] A. Donnachie and P.V. Landshoff, Phys. Lett. **B296** (1992) 227.